The Astrophysical Journal, 804:10 (8pp), 2015 May 1 doi:10.1088/0004-637X/804/1/10
© 2015. The American Astronomical Society. All rights reserved.

A NEARBY M STAR WITH THREE TRANSITING SUPER-EARTHS DISCOVERED BY K2

Ian J. M. Crossfield[1,12], Erik Petigura[2], Joshua E. Schlieder[3,13], Andrew W. Howard[4], B. J. Fulton[4], Kimberly M. Aller[4], David R. Ciardi[5], Sébastien Lépine[6], Thomas Barclay[3], Imke de Pater[2], Katherine de Kleer[2], Elisa V. Quintana[3], Jessie L. Christiansen[5], Eddie Schlafly[7], Lisa Kaltenegger[11], Justin R. Crepp[8], Thomas Henning[7], Christian Obermeier[7], Niall Deacon[9], Lauren M. Weiss[2], Howard T. Isaacson[2], Brad M. S. Hansen[10], Michael C. Liu[4], Tom Greene[3], Steve B. Howell[3], Travis Barman[1], and Christoph Mordasini[7,12]

[1] Lunar & Planetary Laboratory, University of Arizona Lunar, 1629 E. University Blvd., Tucson, AZ, USA; ianc@lpl.arizona.edu
[2] Astronomy Department, University of California, Berkeley, CA, USA
[3] NASA Ames Research Center, Moffett Field, CA, USA
[4] Institute for Astronomy, University of Hawaii, 2680 Woodlawn Drive, Honolulu, HI, USA
[5] NASA Exoplanet Science Institute, California Institute of Technology, 770 S. Wilson Ave., Pasadena, CA, USA
[6] Department of Physics & Astronomy, Georgia State University, Atlanta, GA, USA
[7] Max-Planck Institut für Astronomie, Königstuhl 17, Heidelberg, Germany
[8] Department of Physics, University of Notre Dame, 225 Nieuwland Science Hall, Notre Dame, IN, USA
[9] University of Hertfordshire, College Lane, AL10 9AB, Hatfield, UK
[10] Department of Physics & Astronomy, University of California Los Angeles, Los Angeles, CA, USA
[11] Department of Astronomy, Cornell University, 122 Sciences Drive, Ithaca, NY, USA
[12] Physikalisches Institut, Silderstrasse 5, CH-3012 Bern, Switzerland
Received 2015 January 15; accepted 2015 February 16; published 2015 April 23

ABSTRACT

Small, cool planets represent the typical end-products of planetary formation. Studying the architectures of these systems, measuring planet masses and radii, and observing these planets' atmospheres during transit directly informs theories of planet assembly, migration, and evolution. Here we report the discovery of three small planets orbiting a bright ($K_s = 8.6$ mag) M0 dwarf using data collected as part of K2, the new ecliptic survey using the repurposed *Kepler* spacecraft. Stellar spectroscopy and K2 photometry indicate that the system hosts three transiting planets with radii 1.5–2.1 $R_\oplus$, straddling the transition region between rocky and increasingly volatile-dominated compositions. With orbital periods of 10–45 days the planets receive just 1.5–10× the flux incident on Earth, making these some of the coolest small planets known orbiting a nearby star; planet d is located near the inner edge of the system's habitable zone. The bright, low-mass star makes this system an excellent laboratory to determine the planets' masses via Doppler spectroscopy and to constrain their atmospheric compositions via transit spectroscopy. This discovery demonstrates the ability of K2 and future space-based transit searches to find many fascinating objects of interest.

Key words: eclipses – stars: individual (EPIC 201367065) – techniques: photometric – techniques: spectroscopic

Supporting material: data behind figure, tar.gz file

1. INTRODUCTION

Surveys for new planets demonstrate that small, low-mass planets are common around FGK stars (Howard et al. 2010, 2012). Petigura et al. (2013) used *Kepler* data to measure the frequency of Earth-sized planets in Earth-like orbits to be 5%–20%. Such small planets with moderate insolation levels (the stellar energy received by the planet at the top of any atmosphere) are of considerable interest for their ability to host Earth-like atmospheres that could potentially support life.

M dwarfs offer a shortcut to observing rocky and potentially habitable planets. Compared to nearby Sunlike stars, planets around M dwarfs are easier to find with transits or radial velocities (RV), they occur more frequently (Howard et al. 2012), and their atmospheres are easier to study when transiting (Stevenson et al. 2010; Kreidberg et al. 2014). Planets transiting M dwarfs offer the best opportunity to study habitability and constrain models of rocky planet assembly and migration (Swift et al. 2013; Hansen 2014) and of planetary atmospheres (Kaltenegger et al. 2011; Rodler and López-Morales 2014). Multi-planet M dwarf systems are even more exciting, both because such candidates are extremely unlikely to result from astrophysical false positives (Lissauer et al. 2012) and because they allow for studies of comparative planetology (Muirhead et al. 2012) with identical initial conditions (i.e., formation in the same natal disk). However, relatively few confirmed transiting planets (and fewer multiple systems) are known around M dwarfs, and (because *Kepler*'s prime mission targeted just 3900 late-type dwarfs) the prevalence of planets around M dwarfs is less well constrained than around Sunlike stars (Dressing & Charbonneau 2013).

We are using K2, the continuing mission of NASA's *Kepler* spacecraft (Howell et al. 2014), to target thousands of M dwarfs in each K2 field to find new, small planets orbiting these stars. K2's 80 day campaigns are ideally suited to finding large numbers of small, cool planets around M dwarfs, out to semimajor axes in the stars' habitable zones (e.g., Kopparapu et al. 2014). In addition, some of K2's M dwarf planets orbit stars bright enough for atmospheric characterization via *James Webb Space Telescope (JWST)* transmission or emission spectroscopy (Kaltenegger & Traub 2009; Batalha et al. 2013; Beichman et al. 2014).

[12] NASA Sagan Fellow.
[13] NASA Postdoctoral Program Fellow.

Table 1
Stellar Parameters of K2–3

Parameter	Value	Source
Identifying Information		
α R.A. (hh:mm:ss)	11:29:20.388	
δ Decl. (dd:mm:ss)	–01:27:17.23	
EPIC ID	201367065	
2MASS ID	11292037-0127173	2MASS
Photometric Properties		
B (mag).....	13.52 ± 0.06	APASS
V (mag).....	12.17 ± 0.01	APASS
g (mag).....	12.871 ± 0.030	APASS
r (mag).....	11.582 ± 0.020	APASS
i (mag).....	10.98 ± 0.17	APASS
J (mag).....	9.421 ± 0.027	2MASS
H (mag).....	8.805 ± 0.044	2MASS
Ks (mag).....	8.561 ± 0.023	2MASS
$W1$ (mag).....	8.443 ± 0.022	AllWISE
$W2$ (mag).....	8.424 ± 0.019	AllWISE
$W3$ (mag).....	8.322 ± 0.021	AllWISE
Spectroscopic and Derived Properties		
μ_α (mas yr^{-1})	88.3 ± 2.0	Zacharias et al. (2012)
$\mu\delta$ (mas yr^{-1})	-73.6 ± 2.7	Zacharias et al. (2012)
Barycentric rv (km s^{-1})	32.6 ± 1	APF, this paper
Distance (pc)	45 ± 3	This paper
EW (Hα) (Å)	0.38 ± 0.06	EFOSC, this paper
Age (Gyr)	$\gtrsim 1$	EFOSC, this paper
Spectral Type	M0.0 ± 0.5 V	This paper
[Fe/H]	-0.32 ± 0.13	SpeX, this paper
$T_{\rm eff}$ (K)	3896 ± 189	SpeX, this paper
M_* ($M_\odot$)	0.601 ± 0.089	SpeX, this paper
R_* ($R_\odot$)	0.561 ± 0.068	SpeX, this paper

Here, we present the discovery of a new multi-planet system orbiting a bright M dwarf (K2–3, PMI:112911293-0127, UCAC4 443-054906, PPMX 112920.3-012717). We describe our analysis of the K2 photometry and of supplementary imaging and spectroscopic data in Section 2. In Section 3 we present the results of our analysis of K2–3's properties and discuss the potential for future observations of this and other systems discovered by K2.

2. OBSERVATIONS AND ANALYSIS

We identified the high proper motion star PMI 11293-0127 as a target for our Campaign 1 proposal (GO1036[14], PI: I. J. M. Crossfield) from the SUPERBLINK proper motion survey (Lépine & Shara 2005; Lépine & Gaidos 2011). We identified the star as a probable nearby M dwarf based on a color and proper motion selection scheme, selecting all targets with $(V - J) > 2.5$, $V + 5 \log \mu + 5 < 10$, and $(6V - 7J - 3) < 5 \log \mu$, where μ is the proper motion. The star matched the source K2–3 in the *Kepler* input catalog (Huber 2014). K2 then observed this target in long-cadence mode during C1, covering 2014 May 30 to Aug 21. Target properties, including optical and near-infrared (NIR) photometry from APASS (Henden et al. 2012), 2MASS (Skrutskie et al. 2006), and *WISE* (Wright et al. 2010), are summarized in Table 1.

2.1. K2 Photometry

2.1.1. Extracting the Photometry

We extracted the photometry K2–3 from the pixel data, which we downloaded from the MAST. Because K2 only has two functional reaction wheels, the telescope cannot maintain the 50 millipixel pointing precision achieved during the prime mission. Roll is the dominant drift around the telescope boresight. When the spacecraft reaches a pre-determined limit, the spacecraft corrects this roll with a thruster fire. As the spacecraft rolls, stars move over different pixels having different sensitivities. Thus, motion of the star results in apparent changes in stellar brightness.

Because a target star traces out similar paths during each roll of the spacecraft, it is possible to separate out variations in stellar brightness that are roll-angle dependent, and to remove these variations from the photometry. Our extraction pipeline draws heavily on the work of Vanderburg & Johnson (2014). We begin by computing the median flux for each frame and adopt this value as the background flux level. The background flux is subtracted out on a frame by frame basis. We compute the raw photometry, $F_{\rm SAP}$, by summing the flux within a soft-edged circular aperture centered around the target star. We compute the row and column centroids within the aperture.

On short timescales, spacecraft roll is the dominant motion term and can be described by a single variable. We identify the roll direction by computing the principle components of the row and column centroids, x' and y'. We fit for a function that relates $F_{\rm SAP}$ to x'. We describe this trend by $F_{\rm SAP} = {\rm GP}(x')$, where GP is a Gaussian process having a correlation matrix given by a squared exponential kernel. Fitting the GP(x') is an iterative process where outliers are identified and removed and the hyperparameters associated with the squared exponential kernel are adjusted to yield the minimum residual rms.

The algorithm described in Vanderburg & Johnson (2014) was developed for the K2 engineering campaign (C0), where the time baseline was short enough that drifts in a stellar position along the y' direction could be ignored. During the 80 day period of C1 observations, stars moved enough along the y' direction that the GP(x') determined using data early in the campaign was no longer an appropriate description of the position-dependent flux variations. Adopting an approach described in Vanderburg (2014), we divided the C1 observations into six nearly equal segments and performed the 1D decorrelation approach described above on each segment individually. The entire procedure described above is repeated for different aperture radii (2, 3, 4, 5, 6, and 7 pixels). We select the aperture size that minimizes the calibrated rms. For K2–3, a circular aperture with a 4 pixel radius yielded the best calibrated photometry (which is available as an electronic supplement to this paper). Our photometry suggests that K2–3 may exhibit photometric variations of $\lesssim$1% on week to month timescales, but K2's long-term stability is constrained sufficiently poorly that we cannot claim evidence for periodic modulation indicative of stellar rotation.

2.1.2. Transit Detection

We searched through the calibrated and detrended photometry (shown in Figure 1(a)) using the TERRA algorithm

[14] The star was also identified in programs GO 1006, GO 1050, GO 1052, GO 1036, GO 1075, GO 1059, and GO 1063.

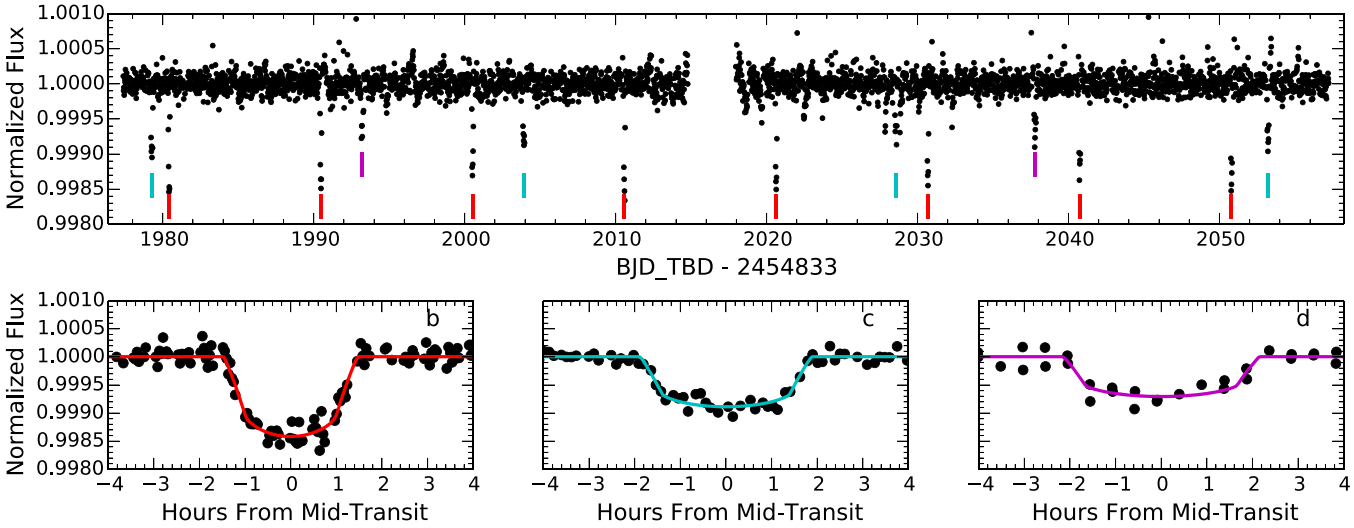

Figure 1. *Top*: calibrated K2 photometry for K2–3. Vertical ticks indicate the locations of each planets' transits. *Bottom*: phase-folded photometry and best-fit light curves for each planet.The data used to create this figure are available.

described in Petigura et al. (2013). TERRA identified a transit candidate having $P = 10.056$ days and signal-to-noise ratio (S/N) = 59. We fit this candidate with a Mandel & Agol (2002) model and subtracted the best fit model from the photometry. We reran TERRA on the photometry with the $P = 10.056$ days candidate removed. We found a second candidate having $P = 24.641$ days and S/N = 30. Again we removed the best-fitting model. TERRA did not find any additional transits, but a ∼45 day candidate was identified by eye (TERRA currently requires three detected transits, and thus was not sensitive to the longest period candidate which only transits twice during C1). We fit each of these two transits individually and find consistent transit parameters, supporting the hypothesis that they result from a single planet. At half of this period a third transit would occur in C1's data gap (see Figure 1), but this would give the outer two planets a period ratio of just 1.1. The previous record-holder for a close period ratio is the Kepler-36 system (Carter et al. 2012; Winn & Fabrycky 2014), whose two planets exhibit a considerably larger period ratio of 1.17 and transit timing variations of many hours. It is unlikely that such an unusual system would lie just 45 pc away; in addition, our dynamical analysis (described below) indicates that this period ratio would be dynamically unstable. We therefore conclude that the third planet's period is ∼45 days.

2.2. Target Validation and Stellar Spectroscopy

We conducted a number of pixel-level diagnostics and observed K2–3 using several spectrographs to constrain the stellar properties. These observations are described below. The reduced spectra are available in the HTML version of the journal, and the derived parameters are listed in Table 1.

2.2.1. Pixel-level and Photometric Data Validation

Experience over the last decade shows that transit-like signals must be validated to ensure that they arise from true planets, not "false-positive" configurations such as background eclipsing binaries blended with foreground stars (e.g., Torres et al. 2004, 2011). We therefore implement a large number of tests on the pixel-level data and extracted photometry to identify and weed out these false positives.

Once transit-like events are identified, TERRA runs a suite of diagnostics to distinguish planets from phenomena like eclipsing binaries, starspots, and other periodic stellar variability. We subject targets passing this first step to an extensive battery of further tests which search for blends using an examination of centroid motions in and out of transit, difference imaging analyses, and construction of pixel correlation images (Bryson et al. 2013). Though we are still learning how to optimally tune these tests to account for K2's few-pixel pointing variations, validation results for large numbers of targets indicate that the transit-like events identified with K2–3 occur within roughly one pixel (4″) of the target star. When combined with our seeing-limited and adaptive optics imaging described below, as described in Section 2.5, we find that K2–3's transits are far more likely to be explained by a multi-planet system than by nonplanetary phenomena.

2.2.2. Optical and Infrared Spectroscopy

We obtained $R \sim 1500$ spectra from 0.6 to 1.0 μm of K2–3 and a number of calibration objects using NTT/EFOSC2 (Buzzoni et al. 1984) on UT 2015 Jan 11 as part of a 70 night *K2* followup program (PID 194.C-0443, PI: I.J.M. Crossfield). We draw our calibrators from several recent works (Boyajian et al. 2012; Mann et al. 2013a; Pecaut & Mamajek 2013). A forthcoming paper will discuss these efforts; in brief, we bias-subtract and flat-field the data frames, extract spectra using IRAF, and wavelength-calibrate using EFOSC2's internal HeAr lamps. We achieve an S/N per resolution element of ∼100 for K2–3 and somewhat higher for our reference sample. We flux-calibrate the extracted spectrum using observations of spectrophotometric standards.

We observed K2–3 on 2015 January 11 UT using the recently refurbished SpeX spectrograph (Rayner et al. 2003) on the 3.0 m NASA Infrared Telescope Facility (IRTF). The data were taken under clear skies with an average seeing of ∼0.″7. We observed with the instrument in short cross dispersed mode (SXD) using the 0.3 × 15″ slit. This setup provides simultaneous wavelength coverage from 0.7 to 2.5 μm at a resolution of $R \approx 2000$. The extended blue wavelength

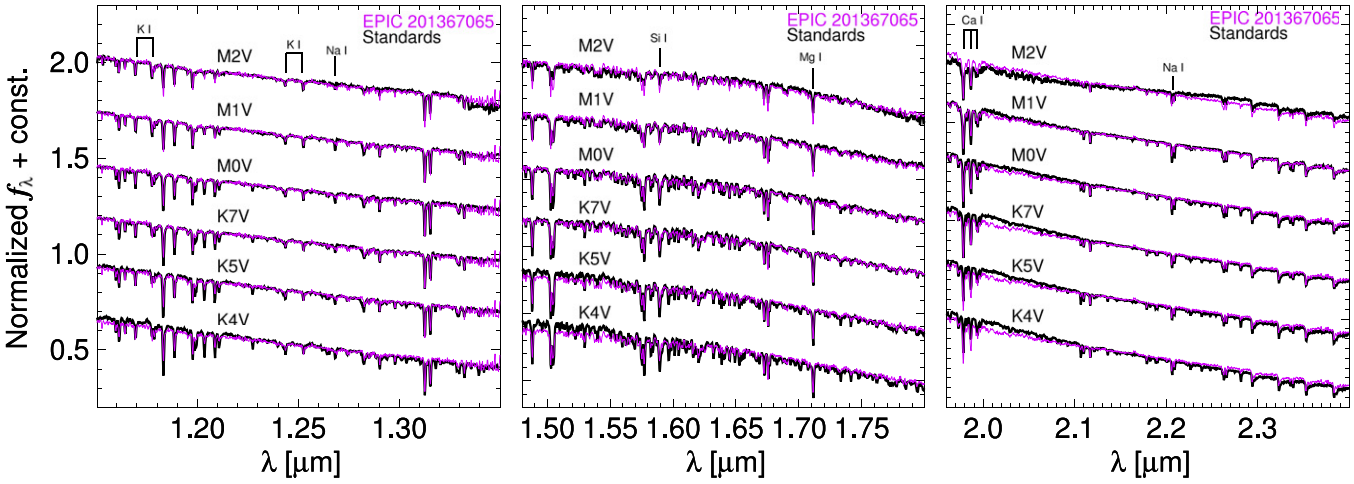

Figure 2. Calibrated IRTF/SpeX spectra of our target compared to spectral standards. Stellar parameters are tabulated in Table 1.

coverage is a result of the recent chip upgrade SpeX received in 2014 July. The target was placed at two positions along the slit and observed in an ABBA pattern for subsequent sky subtraction. The observing sequence consisted of 8 × 40 s exposures for a total integration time of 320 s. Once the exposures were stacked, this integration time led to an S/N of >140 per resolution element. We obtained standard SpeX calibration frames consisting of flats and arc lamp exposures immediately before observing K2–3.

The SpeX spectrum was reduced using the SpeXTool software package (Cushing et al. 2004). SpeXTool performs flat-field correction and wavelength calibration from the calibration frames followed by sky subtraction and extraction of the one-dimensional spectrum. Individual exposures of the target were combined using the *xcombspec* routine within SpeXTool. We corrected for atmospheric absorption and performed flux calibration using the A0V-type star HD 97585 which was observed within 20 minutes and 0.015 airmass of the target. A telluric correction spectrum was constructed from the spectrum of the A0V using the *xtellcor* package (Vacca et al. 2003) and was applied to the spectrum of K2–3. This package also performs flux calibration. Separate, telluric-corrected SpeX orders were combined and flux-matched into a continuous spectrum using the *xmergeorders* routine. To minimize errors in the spectral slope due to changes in seeing, guiding, and differential refraction, we aligned the slit with the parallactic angle and minimized the time between observations of the target and standard star. Prior to performing any spectroscopic analyses, we also applied corrections for the barycentric velocity of the observatory and the measured RV. The final, calibrated spectrum is shown in Figure 2.

2.2.3. Stellar Parameters

Mann et al. (2013b) motivate a set of temperature sensitive spectral indices spanning the visible, J, H, and K bands that are calibrated using the M dwarf sample of Boyajian et al. (2012) with interferometrically measured radii. We used these indices to estimate the temperature of K2–3. We calculate the mean of the temperatures from each of the three NIR band indices and their rms scatter and find $T_{\rm eff}$ = 3896 ± 117 K (±148 K systematic error, ±189 K total error). This range of effective temperatures is consistent with main-sequence M0 dwarfs of spectral type K8V to M0V (Pecaut & Mamajek 2013), using the modified system which incorporates subtypes K8V and K9V between K7V and M0V.

We adopt the metallicity calibration of Mann et al. (2013a) to remain consistent with our methods for determining $T_{\rm eff}$ and other parameters. We use custom IDL software provided by A. Mann[15] to calculate the metallicity in in the visible, J, H, and K bands following the calibrations of Mann et al. (2013a). Since our SpeX spectrum does not extend <0.7 μm, we do not use the visible band calibrations. Following the suggestion of Mann et al. (2013a), we also discard the J-band metallicity, which is often an outlier. Our final metallicity is the mean of those measured from the H- and K-band relations and the error is the quadrature sum of the measurement error and systematic error in each band. We find [Fe/H] = −0.32 ± 0.13. Thus, K2–3's metallicity is sub-solar, broadly consistent with many other nearby, field-age, M dwarfs.

Mann et al. (2013b) provide empirical calibrations to calculate the radii, masses, and luminosities given the $T_{\rm eff}$ of an M dwarf. We estimate these additional fundamental parameters again using IDL software written by A. Mann[16] to calculate radius, mass, and luminosity and their associated errors using the relations detailed in Mann et al. (2013a). Using the most conservative $T_{\rm eff}$ errors, we calculate $R_* = 0.561 \pm 0.068\ R_\odot$ and $M_* = 0.601 \pm 0.089\ M_\odot$. These values, and the other fundamental parameters of the star, are tabulated in Table 1 and are used for subsequent estimates of the individual planet properties.

Independent of these parameters, we also assign a spectral type to this star using molecular band heads in our optical and NIR spectra. In the optical, the TiO5, CaH2, and CaH3 indices (Reid et al. 1995; Gizis 1997) are calibrated for the earliest M dwarfs (Lépine et al. 2003) and avoid regions of the spectrum with heavy telluric contamination. Following the most recent spectral type calibrations of these indices by Lépine et al. (2013), our EFOSC spectrum yields a spectral type of K7.5 ± 0.5, determined to a half-subtype scale and assuming a sequence K5–K7–M0 (i.e., without the K8 and K9 subdivisions of Pecaut & Mamajek 2013). In the NIR, the H_2O–K2 index measures water opacity in the K-band, and was calibrated to a spectral subtype by Rojas-Ayala et al. (2012).

[15] https://github.com/awmann/metal
[16] https://github.com/awmann/Teff_rad_mass_lum

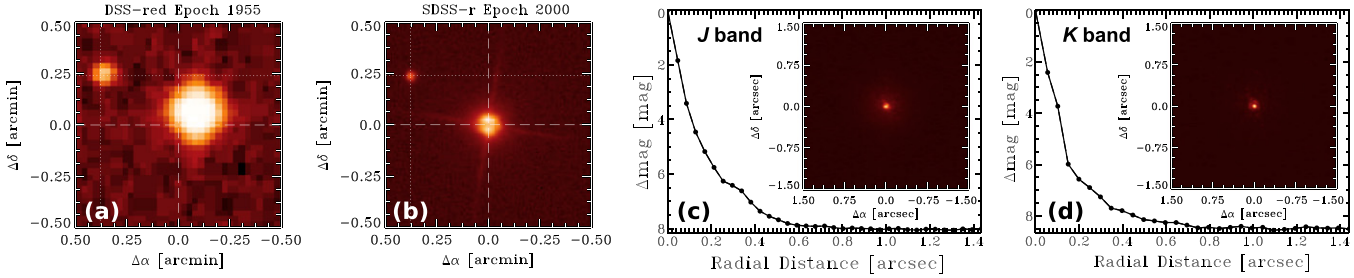

Figure 3. We detect no objects within 25″ of K2–3 in DSS (a) SDSS (b) and with Keck/NIRC2 in J band (c) and K band (d).

We calculate this index from our SpeX spectrum and estimate a spectral type of M0.5 ± 0.5. Lépine et al. (2013) also provide a calibration of the $V - J$ color to spectral subtype. Our target has $V - J = 2.75$, consistent with subtype K7.5 on the scale of Pecaut & Mamajek (2013).

The spectroscopic and photometric classifications are all consistent, although the NIR classification is marginally later. Here we average the optical and infrared results and adopt a spectral type of M0.0 ± 0.5 V. Using the *riJHK* photometric calibrations of Kraus & Hillenbrand (2007), we estimate a distance to K2–3 of 45 ± 3 pc.

We obtained high-resolution (2″ slit width with the B decker) spectra of K2–3 with the Levy Spectrometer (Radovan et al. 2010) on the Automated Planet Finder (APF) telescope (Vogt et al. 2014). The spectra were reduced using standard procedures, as described in Fulton & Sinukoff (2015). Inspection of the gravity-sensitive lines confirms that K2–3 is a high gravity target, consistent with the medium resolution spectra described above. We do not see any evidence of a second set of spectral lines, ruling out companions ∼2.5 mag fainter than K2–3 at visible wavelengths.

2.2.4. Activity, Age, and Membership

Lines in the Balmer series are associated with magnetic activity in late-type stars. The strongest line in the series, Hα at 6563 Å, is classically used to assess the activity of M dwarfs and as a crude indicator of age (West et al. 2004, 2008). We therefore measure the Hα equivalent width (EW) as defined by West et al. (2011) and Lépine et al. (2013) and find consistent results using both approaches. We use two different integration regions to calculate this EW and apply Monte Carlo methods to estimate the uncertainty in the EW measurements. We find that EW = 0.38 ± 0.06 Å, indicating that K2–3 is a relatively inactive star. We further investigate possible chromospheric activity in K2–3 by analyzing its UV emission measured by *GALEX* (Martin et al. 2005). The star is a weak near-UV (NUV) emitter and is not detected in the far-UV (FUV). Its low NUV flux and non-detection in the FUV is consistent with quiescent emission, similar to other nearby field M dwarfs (Shkolnik et al. 2011). The Hα absorption, UV fluxes, and lack of chromospheric activity in an M0 dwarf all indicate an old, field-age star and translate to a lower age limit of ∼1 Gyr (West et al. 2008).

We further examined the possibility that K2–3 is young by comparing its space position (*XYZ*) and kinematics (*UVW*) with those of known young moving groups. Its six-dimensional *UVWXYZ* position is inconsistent with the well-known nearby young (≈10–100 Myr) groups summarized by Gagné et al. (2014), as well as other sparser or slightly older groups (Shkolnik et al. 2009; Zuckerman et al. 2013). To provide a quantitative estimate, we used the BANYAN II web tool (Malo et al. 2013; Gagné et al. 2014). BANYAN II calculates the probability of an object being a member of a nearby young moving group using Bayesian inference and the observed proper motion, sky coordinates, RV, and distance. The probability of K2–3 being a member of one of the known nearby young moving groups is <0.1% given the sky coordinates, proper motion, and RV. Inclusion of the photometric distance estimate (and conservatively assuming a 20% distance uncertainty) does not change the BANYAN II results. Thus we conclude that K2–3 is unlikely to be a member of any of these young moving groups.

2.3. Archival and Adaptive Optics Imaging

To rule out the presence of a background star being the source of or diluting the transit events, we compare two epochs of imaging data from the DSS and the Sloan Digital Sky Survey (SDSS; Ahn et al. 2012) separated by 45 yr. The data shown in Figure 3 are the DSS-red plates with a pixel scale of 1.″7 pixel taken on 1955 April 19 and the SDSS r-band image with a pixel scale of 0.″396 pixel taken on 2000 March 3. The images are 1 arcmin on a side and clearly show the proper motion of the primary target. The nearby star located 27″ to the NE is consistent with zero motion within our astrometric uncertainties; this star lies outside the photometric aperture applied to the K2 photometry. The primary target, in contrast, displays a clear proper motion of 6.″2 over 45 yr, in reasonable agreement with the measured proper motion (Lépine & Gaidos 2011; Zacharias et al. 2012). In the DSS image there is no evidence of a background star, and we estimate if a star is located at the position of the primary target in the *Kepler* data, that star must be at least six magnitudes (or more) fainter than the target star.

NIR adaptive optics imaging of K2–3 was obtained at Keck Observatory on the nights of 2015 January 12 UT and 2015 Janary 16 UT. Observations were obtained with the 1024 × 1024 NIRC2 array and the natural guide star system; the target star was bright enough to be used as the guide star. The data were acquired in the narrow-band K-band and J-band continuum filters (Kcont and Jcont) using the narrow camera field of view (FOV) with a pixel scale of 9.942 mas pix^{-1}; the atmosphere was less stable on night 1 and only Kcont was acquired on that night. A three-point dither pattern was utilized to avoid the noisier lower left quadrant of the NIRC2 array. For both nights, the three-point dither pattern was observed with 10 coadds and a 1.5 integration time, but on night 1 only four frames were acquired for a total of 60 s of on-source exposure time. For night 2, three full dither patterns were acquired for a total on-source exposure time of 135 s in both Kcont and Jcont filters. The data from each night were flat-fielded and sky-

subtracted and the dither positions were shifted and coadded into a single final image. The final images from night 2 are shown in Figures 3(c) and (d).

For night 1, the target star was measured with a resolution of 0.″07 (FWHM), but the atmosphere was much more stable during night 2 and these images have a resolution of 0.″05 in the Kcont filter and 0.″04 in the Jcont filter. No other stars were detected within the 10″ FOV of the camera; speckles seen in the Kcont images are not co-spatial with the speckles seen in the Jcont image, indicating that the speckles are not faint companions. The night 2 data were much more sensitive than the night 1 data and we report the analysis of those data in this work. In the Kcont filter, the data are sensitive to stars that have a K-band brightness of Δmag = 2.4 mag at a separation of 0.″05 and Δmag = 8.0 mag at a separation of 0.″5 from the central star; in the Jcont filter, the data are sensitive to stars that have a J-band brightness of Δmag = 2.0 mag at a separation of 0.″05 and Δmag = 7.5 mag at a separation of 0.″5 from the central star (see Figures 3(c) and (d)). We estimate the sensitivities by injecting fake sources with an S/N of 5 into the final combined images at distances of N*FWHM from the central source. The 5σ sensitivities, as a function of radius from the star are shown in Figures 3(c) and (d).

2.4. Light Curve Fitting

We analyze the photometry using standard Python-based minimizers, the `emcee` Markov Chain Monte Carlo (MCMC) package (Foreman-Mackey et al. 2013), and the JKTEBOP light curve code (Southworth et al. 2004; Southworth 2011) using numerical integration to account for our ~30 minute cadence. We fit each planet's transit separately, after first masking out data taken during the other planets' transits.

We use the best-fit TERRA parameters to initialize the fits. We assumed a linear limb-darkening relation for the star. Because the data are insufficient to break all degeneracies between the light curve parameters (Muirhead et al. 2012), we impose Gaussian priors in our analysis. For the limb-darkening parameter u, we assume a distribution with center 0.560 and dispersion 0.044; these values correspond to the mean and standard deviation, respectively, of all linear limb-darkening terms tabulated by (Claret et al. 2012) that satisfy $3300 \leqslant T_{\rm eff} \leqslant 3700$ K and $\log_{10} g \geqslant 4.5$. Using the spectroscopic parameters presented below (Table 1), we also impose a prior on the stellar density to constrain R_*/a (Seager & Mallén-Ornelas 2003). This last point assumes that the planets' orbits are circular, an assumption that future RV measurements will test.

We seed our 60 MCMC chains with values near the best-fit parameters. We assign our data points equal weights, such that the best-fit likelihood equals $-\chi^2/2$. After burn-in we run the MCMC sampler: after each set of 2000 steps, we optimize the fits given by each chain's parameters to check for better fits to the data. We re-initialize the sampler and re-scale the data weights if we find an improved fit, repeating until all parameters' chains are well-mixed (as indicated by Gelman-Rubin metrics $\leqslant$1.03; Gelman & Rubin 1992). As our final confidence intervals, we use the 15.87% and 84.13% percentiles of each parameters' posterior distribution. The final distributions are unimodal. Figure 1 shows the resulting photometry and best-fit models, and Table 2 summarizes the final values and uncertainties.

2.5. Ruling Out False Positives

Almost all candidates in *Kepler*'s multi-planet systems are *bona fide* planets (Lissauer et al. 2011), but one pernicious source of confusion is the possibility of mistaking blended stars each hosting their own planets for a single multi-planet system. We therefore investigated the possibility that K2–3 might be a blend of multiple stars. First, we note that K2–3's proper motion (listed in Table 1) is large enough that optical DSS survey images reveal no objects at the star's current location (see Figures 3(a) and (b)). Our Keck/NIRC2 images also show no companions at separations down to a fraction of an arc second (see Figures 3(c) and (d)), and so our data validation tests indicate that the transits must occur around K2–3 and not around some other nearby star. Blends involving background eclipsing binaries are thus strongly disfavored.

The most likely remaining false positive configuration involves a heirarchical triple system, with a later-type M dwarf close to K2–3 and with its own transiting planet(s)—but this too is extremely unlikely. An M4 dwarf would have $\Delta K_p \approx 2.7$ and so might be missed in our APF and EFOSC spectra, but the M4 would have $\Delta K_s \approx 2.0$ (Kraus & Hillenbrand 2007) and so to avoid detection in our Keck/NIRC2 image it would need to lie at $a \lesssim 2.3$ AU—while still needing to host its own 2 $R_\oplus$ transiting planet. The likelihood that K2–3 has such a low-mass stellar companion is ~0.4 and that such a companion would lie at a projected separation <2.3 AU is ~0.5 (Duchêne & Kraus 2013). For planet b, the likelihood of an M dwarf hosting such a planet is $\lesssim$0.15 (Dressing & Charbonneau 2013), and the likelihood of it transiting is ~0.02. Then the likelihood of such a contrived configuration is just $\sim 6 \times 10^{-4}$ (1 in 1700), so we eliminate this scenario as well—in any case, such a binary would be quickly revealed by even crude RV measurements. We therefore conclude that K2–3 indeed hosts a three-planet system.

2.6. System Stability

Here we investigate the dynamical stability of the three-planet K2–3 system. The planet masses are unconstrained by transit photometry, so we adopt the following mass–radius relationship:

1. $M = \frac{4\pi}{3} R^3 \rho$, where $\rho = (2.43 + 3.39 * (R_P/R_\oplus))$ g cm^{-3} for $R_P < 1.5\ R_\oplus$ (Weiss & Marcy 2014).
2. $M = 2.69\ M_\oplus \left(\frac{R_P}{R_\oplus}\right)^{0.93}$ (Weiss & Marcy 2014) for $1.5\ R_\oplus < R_P < 4.0\ R_\oplus$.
3. $M = M_\oplus \left(\frac{R_P}{R_\oplus}\right)^{2.06}$ for $R_P > 4.0\ R_\oplus$ (Lissauer et al. 2012).

Adopting the above mass–radius relationship we derive masses of 5.3, 4.3, and 4.4 $M_\oplus$ for planets b, c, and d, respectively. We integrate the system forward in time with the Mercury integration package (Chambers 1999) utilizing the hybrid integrator and found the system to be stable for the full 2×10^5 yr simulation.

We also evaluate analytically the system's stability. The relevant length scale for dynamical interactions between planets is the mutual Hill radius

$$R_H = \left[\frac{M_{\rm in} + M_{\rm out}}{3M_\star}\right]^{1/3} \frac{a_{\rm in} + a_{\rm out}}{2} \quad (1)$$

Table 2
Planet Parameters

Parameter	Units	b	c	d
T_0	$BJD_{TDB} - 2454833$	$1980.4189^{+0.0011}_{-0.0011}$	$1979.2786^{+0.0026}_{-0.0027}$	$1993.2232^{+0.0037}_{-0.0043}$
P	day	$10.05403^{+0.00026}_{-0.00025}$	$24.6454^{+0.0013}_{-0.0013}$	$44.5631^{+0.0063}_{-0.0055}$
i	deg	$89.28^{+0.46}_{-0.60}$	$89.55^{+0.29}_{-0.44}$	$89.68^{+0.21}_{-0.26}$
R_P/R_*	%	$3.483^{+0.123}_{-0.070}$	$2.786^{+0.143}_{-0.083}$	$2.48^{+0.14}_{-0.10}$
T_{14}	hr	$2.553^{+0.047}_{-0.044}$	$3.428^{+0.106}_{-0.097}$	$3.98^{+0.17}_{-0.15}$
R_*/a	–	$0.0343^{+0.0049}_{-0.0020}$	$0.0193^{+0.0041}_{-0.0014}$	$0.0127^{+0.0025}_{-0.0010}$
b	–	$0.37^{+0.22}_{-0.23}$	$0.41^{+0.26}_{-0.25}$	$0.45^{+0.23}_{-0.28}$
u	–	$0.560^{+0.041}_{-0.042}$	$0.557^{+0.043}_{-0.044}$	$0.563^{+0.041}_{-0.042}$
a	AU	$0.0769^{+0.0036}_{-0.0040}$	$0.1399^{+0.0066}_{-0.0073}$	$0.2076^{+0.0098}_{-0.0108}$
R_P	$R_\oplus$	$2.14^{+0.27}_{-0.26}$	$1.72^{+0.23}_{-0.22}$	$1.52^{+0.21}_{-0.20}$
S_{inc}	$S_\oplus$	$11.0^{+4.1}_{-3.1}$	$3.32^{+1.25}_{-0.95}$	$1.51^{+0.57}_{-0.43}$
T_{eq}	K	~500	~400	~300

where M and a denote mass and semi-major axis, respectively. The subscripts "in" and "out" correspond to the inner and outer planets, respectively. Following Fabrycky et al. (2012), for each pair of planets, we compute $\Delta = (a_{out} - a_{in})/R_H$, the separation between the planets measured in units of their mutual Hill radii. If two planets begin on circular orbits, they are stable indefinitely if $\Delta > 2\sqrt{3} \approx 3.5$ (Gladman 1993). In the case of K2–3, $\Delta_{bc} = 15.9$ and $\Delta_{cd} = 11.0$. Thus, the two pairs of adjacent planets do not violate the criterion of Hill stability.

There is no analytic stability criterion for systems having three or more planets (Fabrycky et al. 2012). Fabrycky et al. (2012) introduce $\Delta_{in} + \Delta_{out}$ as a heuristic metric for assessing the stability of three planets in triple or higher multiplicity systems. They adopt $\Delta_{in} + \Delta_{out} > 18$ as a heuristic criterion for the stability of three planets, motivated by suites of direct numerical integrations (e.g., Smith & Lissauer 2009). This criterion is empirically supported by the ensemble of systems with three or more transiting planets from the *Kepler* mission. Among the 413 such systems in Fabrycky et al. (2012), only six had $\Delta_{in} + \Delta_{out} < 18$. For K2–3, $\Delta_{bc} + \Delta_{cd} = 26.9$, and thus has a similar architecture to the ensemble of triple and higher systems discovered during the prime *Kepler* mission.

3. DISCUSSION

Our analysis indicates three small planets orbiting this bright, nearby M dwarf. The planets range in size from 2 to 1.5 $R_\oplus$, indicating that they may span the gap between rock-dominated "Earths"/"super-Earths" and low-density "sub-Neptunes" with considerable volatile content (Dressing et al. 2014; Marcy et al. 2014; Rogers 2014).

The planets' radii imply masses of roughly 4–5 M_E and Doppler amplitudes of 1.2–2.3 m s^{-1}, within reach of modern RV spectrographs. These mass estimates assume that the planets fall on the mean mass–radius relationship, characterized by high densities and rocky compositions for planets smaller than ~1.6 R_E. However, most of the planets with measured masses and $R_p < 1.6\,R_E$ have high incident fluxes (e.g., Batalha et al. 2011; Howard et al. 2013; Pepe et al. 2013). The mass–radius relationship is poorly constrained for cool planets that are less likely to be sculpted by thermal evolution and photo-evaporation (Lopez et al. 2012). Characterizing the mass–radius relationship for these cool, small planets is an important step in learning whether Earth-size planets in the habitable zone also have Earth-like atmospheres.

The planets receive insolation levels (S_{inc}) of roughly 11, 3.3, and 1.5× that of the Earth for planets b, c, and d, respectively. Planet d is located at the inner edge of the system's habitable zone, with $S_{inc} = 1.51^{+0.57}_{-0.47} S_\oplus$—close to the limits of the empirical habitable zone (e.g., Kopparapu et al. 2014)—making this planet a very interesting potential super-Venus or super-Earth. Because this system is so close the atmosphere of this planet can be explored in the near future; depending on atmospheric, cloud, and surface properties liquid water could potentially persist on planet c (Zsom et al. 2013), but see Kasting et al. (2014).

The K2–3 system is a convenient system to measure the atmospheric properties of small, cool planets. Indeed, the star is a full magnitude brighter than Kepler-138 (Kipping et al. 2014), the previous best system for characterizing cool, nearly Earth-size planets. For cloud-free, hydrogen-dominated atmospheres, we estimate that these planets will show spectral features with amplitudes of $10\,H\,R_p/R_\star^2$ on the order of 100–200 ppm (Miller-Ricci et al. 2009), where H is the atmospheric scale height. These features would be detectable with current instrumentation on the *Hubble Space Telescope* (Kreidberg et al. 2014). Transit features in a heavy atmosphere (e.g., N_2, CO_2) would be an order of magnitude smaller, and secondary eclipses will have depths on the order of $(R_p/R_\star)^2 T_{eq}/T_\star \sim 50$–150 ppm—either of these scenarios should be detectable with *JWST*. By allowing us to measure the masses and atmospheric conditions for three small planets in a single system, K2–3 represents an exciting opportunity to test theories of planet formation and evolution in a single extrasolar laboratory.

That K2 should reveal such a system in its first full campaign demonstrates that the mission will extend *Kepler*'s compelling scientific legacy for years to come. Along with HIP 116454 (Vanderburg et al. 2014), the discovery of K2–3 shows that K2 is already finding fascinating new targets for observation with *JWST* and heralds an era of further unprecedented discoveries in the *TESS* era.

We thank Geoff Marcy, Evan Sinukoff, and Charles Beichman for helpful conversations; Vishnu Reddy for swapping SpeX time; and Steve Bryson and our referee Don Pollacco for useful comments that improved the quality of this manuscript. A. W.H. acknowledges NASA grant No. NNX12AJ23G, and S.L.

acknowledges NSF grant No. AST 09-08419. This work made use of the SIMBAD database (operated at CDS, Strasbourg, France); NASA's Astrophysics Data System Bibliographic Services; the Authorea collaborative writing website; the NASA Exoplanet Archive; and Infrared Science Archive, and data products from the Two Micron All Sky Survey (2MASS), the APASS database, the SDSS-III project, the Digitized Sky Survey, and the *Wide-Field Infrared Survey Explorer*. Portions of this work were performed at the California Institute of Technology under contract with the National Aeronautics and Space Administration. Some of the data presented herein were obtained at the W. M. Keck Observatory (which is operated as a scientific partnership among Caltech, UC, and NASA) and at the Infrared Telescope Facility (IRTF, operated by UH under NASA contract NNH14CK55B). The authors wish to recognize and acknowledge the very significant cultural role and reverence that the summit of Mauna Kea has always had within the indigenous Hawaiian community. We are most fortunate to have the opportunity to conduct observations from this mountain.

Facilities: APF (Levy), IRTF (SPEX), Keck: II (NIRC2), *Kepler*, NTT (EFOSC2)

REFERENCES

Ahn, C. P., Alexandroff, R., Allende Prieto, C., et al. 2012, ApJS, 203, 21
Batalha, N., Kalirai, J., Lunine, J., Clampin, M., & Lindler, D. 2013, Transiting Exoplanet Simulations with the *James Webb Space Telescope*, Tech. Rep., http://www.stsci.edu/jwst/doc-archive/white-papers/JWSTNirspec_BatalhaFinal.pdf
Batalha, N. M., Borucki, W. J., Bryson, S. T., et al. 2011, ApJ, 729, 27
Beichman, C., Benneke, B., Knutson, H., et al. 2014, arXiv:1411.1754
Boyajian, T. S., von Braun, K., van Belle, G., et al. 2012, ApJ, 757, 112
Bryson, S. T., Jenkins, J. M., Gilliland, R. L., et al. 2013, PASP, 125, 889
Buzzoni, B., Delabre, B., Dekker, H., et al. 1984, Msngr, 38, 9
Carter, J. A., Agol, E., Chaplin, W. J., et al. 2012, Sci, 337, 556
Chambers, J. E. 1999, MNRAS, 304, 793
Claret, A., Hauschildt, P. H., & Witte, S. 2012, A&A, 546, A14
Cushing, M. C., Vacca, W. D., & Rayner, J. T. 2004, PASP, 116, 362
Dressing, C. D., & Charbonneau, D. 2013, ApJ, 767, 95
Dressing, C. D., Charbonneau, D., Dumusque, X., et al. 2015, ApJ, 800, 135
Duchêne, G., & Kraus, A. 2013, ARA&A, 51, 269
Fabrycky, D. C., Ford, E. B., Steffen, J. H., et al. 2012, ApJ, 750, 114
Foreman-Mackey, D., Hogg, D. W., Lang, D., & Goodman, J. 2013, PASP, 125, 306
Fulton, Weiss., & Sinukoff, et al. 2015, ApJ, submitted
Gagné, J., Lafrenière, D., Doyon, R., Malo, L., & Artigau, É 2014, ApJ, 783, 121
Gelman, A., & Rubin, D. B. 1992, StaSc, 7, 457
Gizis, J. E. 1997, AJ, 113, 806
Gladman, B. 1993, Icar, 106, 247
Hansen, B. M. S. 2015, IJAsB, 14, 267
Henden, A. A., Levine, S. E., Terrell, D., Smith, T. C., & Welch, D. 2012, JAVSO, 40, 430
Howard, A. W., Marcy, G. W., Bryson, S. T., et al. 2012, ApJS, 201, 15
Howard, A. W., Marcy, G. W., Johnson, J. A., et al. 2010, Sci, 330, 653
Howard, A. W., Sanchis-Ojeda, R., Marcy, G. W., et al. 2013, Natur, 503, 381
Howell, S. B., Sobeck, C., Haas, M., et al. 2014, PASP, 126, 398
Huber, D. 2014, K2: Extending *Kepler*'s Power to the Ecliptic. Ecliptic Plane Input Catalog, Tech. Rep. KSCI-19082-007, http://archive.stsci.edu/k2/epic.pdf
Kaltenegger, L., Segura, A., & Mohanty, S. 2011, ApJ, 733, 35
Kaltenegger, L., & Traub, W. A. 2009, ApJ, 698, 519
Kasting, J. F., Kopparapu, R., Ramirez, R. M., & Harman, C. E. 2014, PNAS, 111, 12641
Kipping, D. M., Nesvorný, D., Buchhave, L. A., et al. 2014, ApJ, 784, 28
Kopparapu, R. K., Ramirez, R. M., SchottelKotte, J., et al. 2014, ApJL, 787, L29
Kraus, A. L., & Hillenbrand, L. A. 2007, AJ, 134, 2340
Kreidberg, L., Bean, J. L., Désert, J.-M., et al. 2014, Natur, 505, 69
Lépine, S., & Gaidos, E. 2011, AJ, 142, 138
Lépine, S., Hilton, E. J., Mann, A. W., et al. 2013, AJ, 145, 102
Lépine, S., & Shara, M. M. 2005, AJ, 129, 1483
Lépine, S., Shara, M. M., & Rich, R. M. 2003, AJ, 126, 921
Lissauer, J. J., Fabrycky, D. C., Ford, E. B., et al. 2011, Natur, 470, 53
Lissauer, J. J., Marcy, G. W., Rowe, J. F., et al. 2012, ApJ, 750, 112
Lopez, E. D., Fortney, J. J., & Miller, N. 2012, ApJ, 761, 59
Malo, L., Doyon, R., Lafrenière, D., et al. 2013, ApJ, 762, 88
Mandel, K., & Agol, E. 2002, ApJL, 580, L171
Mann, A. W., Brewer, J. M., Gaidos, E., Lépine, S., & Hilton, E. J. 2013, AJ, 145, 52
Mann, A. W., Gaidos, E., & Ansdell, M. 2013, ApJ, 779, 188
Marcy, G. W., Isaacson, H., Howard, A. W., et al. 2014, ApJS, 210, 20
Martin, D. C., Fanson, J., Schiminovich, D., et al. 2005, ApJL, 619, L1
Miller-Ricci, E., Seager, S., & Sasselov, D. 2009, ApJ, 690, 1056
Muirhead, P. S., Johnson, J. A., Apps, K., et al. 2012, ApJ, 747, 144
Pecaut, M. J., & Mamajek, E. E. 2013, ApJS, 208, 9
Pepe, F., Cameron, A. C., Latham, D. W., et al. 2013, Natur, 503, 377
Petigura, E. A., Howard, A. W., & Marcy, G. W. 2013, PNAS, 110, 19273
Radovan, M. V., Cabak, G. F., Laiterman, L. H., Lockwood, C. T., & Vogt, S. S. 2010, SPIE 7735, Ground-based and Airborne Instrumentation for Astronomy III, ed. I. S. McLean, S. K. Ramsay, & H. Takami (San Diego, CA: SPIE), 4
Rayner, J. T., Toomey, D. W., Onaka, P. M., et al. 2003, PASP, 115, 362
Reid, I. N., Hawley, S. L., & Gizis, J. E. 1995, AJ, 110, 1838
Rodler, F., & López-Morales, M. 2014, ApJ, 781, 54
Rogers, L. A. 2015, ApJ, in press
Rojas-Ayala, B., Covey, K. R., Muirhead, P. S., & Lloyd, J. P. 2012, ApJ, 748, 93
Seager, S., & Mallén-Ornelas, G. 2003, ApJ, 585, 1038
Shkolnik, E., Liu, M. C., & Reid, I. N. 2009, ApJ, 699, 649
Shkolnik, E. L., Liu, M. C., Reid, I. N., Dupuy, T., & Weinberger, A. J. 2011, ApJ, 727, 6
Skrutskie, M. F., Cutri, R. M., Stiening, R., et al. 2006, AJ, 131, 1163
Smith, A. W., & Lissauer, J. J. 2009, Icar, 201, 381
Southworth, J. 2011, MNRAS, 417, 2166
Southworth, J., Maxted, P. F. L., & Smalley, B. 2004, MNRAS, 351, 1277
Stevenson, K. B., Harrington, J., Nymeyer, S., et al. 2010, Natur, 464, 1161
Swift, J. J., Johnson, J. A., Morton, T. D., et al. 2013, ApJ, 764, 105
Torres, G., Fressin, F., Batalha, N. M., et al. 2011, ApJ, 727, 24
Torres, G., Konacki, M., Sasselov, D. D., & Jha, S. 2004, ApJ, 614, 979
Vacca, W. D., Cushing, M. C., & Rayner, J. T. 2003, PASP, 115, 389
Vanderburg, A. 2014, arXiv:1412.1827
Vanderburg, A., & Johnson, J. A. 2014, PASP, 126, 948
Vanderburg, A., Montet, B. T., Johnson, J. A., et al. 2014, arXiv:1412.5674
Vogt, S. S., Radovan, M., Kibrick, R., et al. 2014, PASP, 126, 359
Weiss, L. M., & Marcy, G. W. 2014, ApJL, 783, L6
West, A. A., Hawley, S. L., Bochanski, J. J., et al. 2008, AJ, 135, 785
West, A. A., Hawley, S. L., Walkowicz, L. M., et al. 2004, AJ, 128, 426
West, A. A., Morgan, D. P., Bochanski, J. J., et al. 2011, AJ, 141, 97
Winn, J. N., & Fabrycky, D. C. 2014, ARAA, submitted
Wright, E. L., Eisenhardt, P. R. M., Mainzer, A. K., et al. 2010, AJ, 140, 1868
Zacharias, N., Finch, C. T., Girard, T. M., et al. 2012, yCat, 1322, 0
Zsom, A., Seager, S., de Wit, J., & Stamenković, V. 2013, ApJ, 778, 109
Zuckerman, B., Vican, L., Song, I., & Schneider, A. 2013, ApJ, 778, 5